**Geoscientific
Model Development**

First description of the Minnesota Earth System Model for Ocean biogeochemistry (MESMO 1.0)

K. Matsumoto[1], K. S. Tokos[1], A. R. Price[2], and S. J. Cox[2]

[1]Department of Geology and Geophysics, University of Minnesota, Minneapolis, USA
[2]School of Engineering Sciences, University of Southampton, Southampton, UK

Abstract. Here we describe the first version of the Minnesota Earth System Model for Ocean biogeochemistry (MESMO 1.0), an intermediate complexity model based on the Grid ENabled Integrated Earth system model (GENIE-1). As with GENIE-1, MESMO has a 3D dynamical ocean, energy-moisture balance atmosphere, dynamic and thermodynamic sea ice, and marine biogeochemistry. Main development goals of MESMO were to: (1) bring oceanic uptake of anthropogenic transient tracers within data constraints; (2) increase vertical resolution in the upper ocean to better represent near-surface biogeochemical processes; (3) calibrate the deep ocean ventilation with observed abundance of radiocarbon. We achieved all these goals through a combination of objective model optimization and subjective targeted tuning. An important new feature in MESMO that dramatically improved the uptake of CFC-11 and anthropogenic carbon is the depth dependent vertical diffusivity in the ocean, which is spatially uniform in GENIE-1. In MESMO, biological production occurs in the top two layers above the compensation depth of 100 m and is modified by additional parameters, for example, diagnosed mixed layer depth. In contrast, production in GENIE-1 occurs in a single layer with thickness of 175 m. These improvements make MESMO a well-calibrated model of intermediate complexity suitable for investigations of the global marine carbon cycle requiring long integration time.

1 Introduction

Earth system Models of Intermediate Complexity (EMICs) occupy a unique and important position within the hierarchy of climate models (Claussen et al., 2002). In many ways, EMICs represent a compromise between high resolution, comprehensive coupled models of atmospheric and oceanic circulation, which require significant computational resources, and conceptual (box) models, which are computationally very efficient but represent the climate system in a highly idealized manner. A critical difference between comprehensive coupled models and box models is the absence of dynamical feedbacks in the latter. In box models, large scale circulation is typically prescribed and not allowed to change over the course of a simulation. The lack of dynamical feedbacks makes box models unsuitable for realistic simulations of transient climate change. On the other hand, comprehensive coupled models are so computationally intensive that their behavior within a given parameter space is difficult to fully explore. EMICs nicely fill this gap by retaining important dynamics while remaining computationally efficient, which is typically achieved by reducing spatial resolution and/or number of processes compared to high resolution coupled models.

The effectiveness of EMICs is evident in the numerous publications that have successfully employed them in studying past, present, and future climates (Ganopolski and Rahmstorf, 2001; Ganopolski et al., 1998; Joos et al., 1999; Knutti et al., 2002; Nusbaumer and Matsumoto, 2008; Plattner et al., 2001). Also, the important role that EMICs played in understanding the postindustrial carbon cycle changes is highlighted in the two recent IPCC science reports TAR (Houghton et al., 2001) and AR4 (IPCC, 2007).

Here we document development of the first version of the Minnesota Earth System Model for Ocean biogeochemistry (MESMO 1.0) based on an existing and successful EMIC called GENIE-1. Our immediate motivation for this work is to possess a tool to investigate postindustrial changes in the natural ocean carbon cycle. Our efforts were thus geared toward improving representation of marine biogeochemistry and distributions of natural and anthropogenic transient tracers in the oceans. These improvements, combined with a

Table 1. Physical model parameters.

Parameter	GENIE-1	MESMO Control	Target-tuned
isopycnal diffusion ($m^2\,s^{-1}$)	4489	4467	
diapycnal diffusion ($m^2\,s^{-1}$)			
upper ocean	$.272\times10^{-4}$	$.74\times10^{-4}$	$.115\times10^{-4}*$
deep ocean	"	"	$1.16\times10^{-4}*$
friction timescale (d)	2.940	2.211	
wind scale	1.932	2.028	
temperature diffusion amplitude ($m^2\,s^{-1}$)	4.67×10^6	3.27×10^6	
temperature diffusion width (radians)	1.083	0.979	
temperature diffusion slope	0.0633	0.1700	
moisture diffusion ($m^2\,s^{-1}$)	1.10×10^6	1.70×10^6	
temperature advection coefficient	0.1122	0.0023	
moisture advection coefficient	0.2270	0.2252	
freshwater flux adjustment (Sv)	0.2264	0.2865	0.3581
sea ice diffusion (m^2s^{-1})	6200	5579	

* GENIE-1 parameters from Edwards and Marsh (2005). Control parameters from NGSA-II tuning exercise. In target tuning, vertically constant vertical diffusivity is modified according to Eq. (1).

more highly resolved upper ocean and reasonable seasonal sea ice formation, represent significant steps toward reaching our immediate objective and making MESMO useful for future investigations of the global ocean carbon cycle. The entire MESMO code is available in Supplemental Materials.

2 A brief description of GENIE-1 relevant for MESMO

GENIE is a new EMIC developed primarily in the UK (http://www.genie.ac.uk/) with the goal of making it as modular as possible so that in theory one can choose to construct a model with any permutation of the existing modules (e.g., slab or 3-D dynamical ocean module coupled to energy balance or 3D dynamical atmospheric module). Following Ridgwell et al. (2007), we will refer to GENIE-1 as a model configuration that consists of the physical climate module C-GOLDSTEIN, a simple atmospheric chemistry module ATCHEM, and a marine biogeochemistry module BIOGEM. As described by Edwards and Marsh (2005), C-GOLDSTEIN is itself a stand-alone, coarse gridded, efficient climate model that is comprised of a 3-dimensional circulation model of the world ocean, an energy and moisture balance model of the atmosphere, and a dynamic and thermodynamic model of sea ice. The ocean model is on a 36×36 equal-area horizontal grid with $10°$ increments in longitude and uniform in sine of latitude; latitude spacing increases from about $3°$ at the equator to about $20°$ at the poles. There are 8 levels in the vertical with the top layer being 175 m thick. Ocean dynamics is based on the thermocline or planetary geostrophic equations with the addition of a linear drag term in the horizontal equations. The resulting "frictional geostrophic" equations (Ed-

wards et al., 1998) are therefore similar to classical general circulation models with momentum acceleration and advection neglected. The model includes the Gent-McWilliams (GM) eddy mixing parameterization according to Griffies (1998) that reduces excessive vertical mixing in coarse gridded models (Duffy et al., 1997; England and Rahmstorf, 1999). The momentum flux that drives the surface ocean circulation is based on the annual NCEP reanalysis wind stress and therefore has no seasonality.

The atmospheric component of C-GOLDSTEIN is an energy and moisture balance model following Weaver et al. (2001). External forcing by shortwave solar radiation is temporally constant, annually averaged and thus has no seasonality. Without explicit atmospheric dynamics, eddy diffusion coefficients of heat and moisture become important in determining the atmospheric distributions of temperature and humidity, both prognostic variables in the model.

Edwards and Marsh (2005) identify twelve underconstrained yet critical parameters, including the two eddy diffusion coefficients in the atmosphere, that largely determine the climate state of C-GOLDSTEIN (Table 1). Through a large ensemble of 2000-year C-GOLDSTEIN simulations where the values of the twelve parameters are randomly changed within specified ranges, they determined a set of parameter values that minimizes the misfit between observations and simulations of surface air temperature and humidity and ocean temperatures and salinities. This exercise gives a degree of objectivity to tuning and credibility to the model.

To this physical model C-GOLDSTEIN, Ridgwell et al. (2007) coupled ATCHEM and BIOGEM, making GENIE-1 a global model of carbon and climate. The

production scheme of BIOGEM is based on Michaelis-Menton type phosphate (PO_4) uptake kinetics, modified by the availability of light and sea ice. The partitioning of uptake into two thirds dissolved phase and one third particulate organic phase follows the Ocean Carbon cycle Model Intercomparison Project Phase 2 (OCMIP-2) BIOTIC protocol (Najjar et al., 2007; Najjar and Orr, 1999). An important advance made by Ridgwell et al. (2007) is the objective calibration of BIOGEM through data assimilation of PO_4 and alkalinity (ALK). GENIE-1 thus benefited from having C-GOLDSTEIN and BIOGEM both calibrated objectively.

3 Rationale for improving GENIE-1

In recent years, GENIE-1 has been used increasingly in climate and carbon cycle studies of the present, future, and past (Lenton et al., 2007; Lenton et al., 2006; Matsumoto, 2007; Ridgwell, 2007; Ridgwell et al., 2007). Also, the computational efficiency of GENIE-1 has allowed it to sweep entire parameter spaces with respect to the Atlantic meridional overturning circulation (MOC) so that the model's MOC behavior is now fairly well characterized (Marsh et al., 2004).

We have been motivated to build on the success of GENIE-1 for a number of reasons, especially when we begin to consider the response of marine biology to climate change. First, the 175 m top layer of the ocean model is too thick compared to typical depths of the euphotic zone and mixed layer in the ocean. This prevents a more realistic representation of marine production for example, because nutrient uptake cannot be given a dependence on the mixed layer depth. The importance of this dependence was shown in a seminal work by Sverdrup (1953). Also, the large vertical gradients of nutrients observed today in the upper ocean are completely lost in the 175 m thick layer such that it is not clear what "surface" nutrient concentration in GENIE-1 really means.

Second, there is still significant room to improve the transient tracer uptake in GENIE-1. The model-predicted 1994 global ocean inventories of CFC-11 is 0.88×10^9 mol and anthropogenic carbon is 171 Pg C (Ridgwell et al., 2007). The corresponding observational estimates based on WOCE and JGOFS surveys are much lower at $0.55 \pm 0.08 \times 10^9$ mol CFC-11 (Willey et al., 2004) and 118 ± 19 Pg C (Sabine et al., 2004). If we consider the roughly +7% systematic bias in the anthropogenic carbon inventory (Matsumoto and Gruber, 2005), the overestimation of this transient tracer uptake by GENIE-1 is even more significant. While these uptakes reflect excessive intermediate water ventilation in GENIE-1, there also needs to be a good match in the deep ocean ventilation.

This brings us to the third reason, which is that the deep ocean ventilation of GENIE-1 ought to be validated with the observed abundance of natural radiocarbon (^{14}C). A community-wide OCMIP-2 study that compared 19 ocean carbon cycle models used deep ocean radiocarbon as a metric to evaluate the models (Matsumoto et al., 2004). This metric has since been used in subsequent descriptions of new carbon cycle models (Muller et al., 2006; Schmittner et al., 2005) and is arguably the most effective means to evaluate ocean models with respect to deep ocean circulation.

The final motivation for improving GENIE-1 is to incorporate as much seasonality as possible. The simplicity of GENIE-1 with the momentum and radiation forcings being annual averages makes the model more appropriate for seeking mean climate states in long term integrations. Examples include studies of the geologic past to document changes in marine sedimentation (Chikamoto et al., 2008; Ridgwell, 2007). For postindustrial changes, the presence of seasonality adds more credibility in general and helps achieve more realistic processes such as seasonal production and formation of polar sea ice.

4 Description of MESMO

The starting point of our model development is Version 6 of CB-GOLDSTEIN (Ridgwell et al., 2007), the non-modular version of GENIE-1. MESMO is identical to Version 6 unless noted otherwise. We decided not to use the word "GENIE" in our model name so as to avoid confusion with the ongoing efforts of the GENIEfy project to develop various flavors of GENIE. The GENIEfy project uses its SVN-controlled code and aims to modularize the different model modules, neither of which applies to our efforts with MESMO. The Bern 3D ocean model is also derived from C-GOLDSTEIN and also does not have the descriptor "GENIE" (Muller et al., 2006).

We describe MESMO's physical climate model (Sect. 4.1) first, followed by its biogeochemistry model (Sect. 4.2). In addition to describing the new features and modifications we adopted in MESMO, we will also briefly note two features that we evaluated but ultimately discarded (Sect. 4.3). Our dead-end efforts may be of some interest in future development efforts by other groups.

4.1 New features in MESMO physical model

First, the vertical resolution in the ocean is increased from 8 layers to 16. To allow biological production to depend on changes in stratification, it is preferable to have at least two layers in the euphotic zone above the critical depth where net production is positive. Therefore, we chose a vertical resolution that contains two complete layers in the top 100 m, which we took as the compensation depth (see Sect. 4.2 below). The midpoints of the 16 layers are: 23, 72, 133, 208, 300, 412, 550, 720, 927, 1182, 1494, 1877, 2347, 2923, 3630, and 4497 m. The increased vertical resolution is concentrated in the upper ocean such that the bottom topography in MESMO is very similar to GENIE-1, as shown in Fig. 1 of Ridgwell et al. (2007).

Second, our vertical diffusivity K_v in the ocean is given a depth dependence following Bryan and Lewis (1979). Their K_v profile has much higher values in the deep ocean compared to the upper ocean and is used to this day in GFDL MOM Versions 3 (Pacanowski and Griffies, 1999) and 4 (Griffies et al., 2004). Indeed a number of studies, such as an in situ SF_6 tracer mixing experiment by Ledwell et al. (2000) and analysis of tidal dissipation by Sjoberg and Stigerbrandt (1992), indicate high mixing rates in the deep ocean. In GENIE-1, K_v is constant with depth, which may contribute to excessive transient tracer uptake (Ridgwell et al., 2007). Following Bryan and Lewis (1979), our depth dependent K_v is much greater in the deep ocean than in the upper ocean, with an arctangent transition at 2000 m:

$$K_v(z) = K_{v0} \cdot \left[0.55 + 0.317 \cdot \text{atan} \left(\frac{z-2000}{300} \right) \right], \tag{1}$$

where K_{v0} is the value of K_v at the bottom. Our choice of K_{v0} yields a depth-averaged K_v equal to the NGSA-II value. The upper ocean K_v is set somewhat lower (Table 1) than Bryan and Lewis' value to be consistent with recent observations (Ledwell et al., 1993; Ledwell et al., 1998).

Third, we have activated seasonal variation in the incoming short wave radiation in the existing code. The incoming radiation was held constant to annual mean values in studies using the 8-level ocean in GENIE-1. As shown below, this helps achieve seasonal polar sea ice formation.

In addition, we have made a modification to the GM eddy mixing parameterization. The Griffies (1998) parameterization, which greatly reduces diapycnal leakage by replacing horizontal mixing with mixing along isopycnal surfaces, can lead to negative nutrient concentrations in the top layer of MESMO where isopycnal slopes are large. This causes the BIOGEM CO_2 chemistry code to crash. We found that it was necessary to reduce the ssmax parameter, which defines the maximum square of the isopycnal slope above which horizontal mixing rather than isoneutral mixing is applied, from 10 to 1 (ssmax=1 is equivalent to ~300 m/degree of latitude).

4.2 New features in MESMO biogeochemistry model

First, the dependence of export production, J_{prod}, on light and PO_4 in GENIE-1 was expanded in MESMO to include dependence on temperature, nutrient limitation by nitrate (NO_3) and CO_2(aq), biomass turnover, and mixed layer depth following Doney et al. (2006):

$$J_{prod} = \frac{1}{\tau} \cdot F_T \cdot F_N \cdot F_I \cdot B \cdot \max\{1, \frac{z_c}{z_{ml}}\}, \tag{2}$$

where the optimal nutrient uptake timescale τ is 15 days. Nutrient uptake is set to occur only above a fixed compensation depth z_c of 100 m where photosynthesis is assumed to exceed respiration. For reference, OCMIP-2 protocol uses z_c of 75 m. The ratio of z_c to the mixed layer depth z_{ml} would allow a bloom-like increase in production as the mixed layer

shoals during the spring season, for example. We diagnose z_{ml} in MESMO using the σ_t density gradient (0.125) criterion (Levitus, 1982).

The temperature dependence term is given by:

$$F_T = \frac{T + 2}{T + 10}, \tag{3}$$

where T is temperature (°C) as in HAMOCC (Maier-Reimer, 1993). The temperature dependence allows higher rates of nutrient uptake in warmer waters to account for universally observed temperature dependent metabolic rates. This dependence, analogous to the heuristic Q_{10}=2 relationship, where the rate doubles for every 10°C increase, was evaluated in GENIE-1 before (Matsumoto, 2007) but is a permanent feature of MESMO.

In addition to PO_4 we included NO_3 and CO_2(aq) as possible limiting nutrients:

$$F_N = \min \left\{ \frac{PO_4}{PO_4 + K_{PO_4}}, \frac{NO_3}{NO_3 + K_{NO_3}}, \frac{CO_2(aq)}{CO_2(aq) + K_{CO_2(aq)}} \right\}, \tag{4}$$

where K_{PO_4}, K_{NO_3}, and $K_{CO_2(aq)}$ are half-saturation constants to be determined. Nitrate dependency is needed to examine the impact of increased river runoff of nitrogen over the industrial period in a future study. Another reason to incorporate NO_3 is that it plays a larger role as the limiting nutrient than PO_4 in the modern ocean. Since the ratio of total oceanic inventories of NO_3 to PO_4 is less than the typical elementary stoichiometry of N to P of 16:1 in phytoplankton, NO_3 becomes more limiting on a global scale. Therefore, global production in GENIE-1, which is based only on PO_4, leads to negative NO_3 concentrations at the surface when PO_4 uptake is directly related to NO_3 by the stoichiometry of 16. Export production in GENIE-1 based on PO_4 compared to NO_3 is larger by about 4%. As noted in Sect. 5.2 below, the nutrient limitation in MESMO at this time is effectively entirely due to NO_3. In the future we will add iron as a limiting nutrient, which will make Equation 4 more meaningful.

In the present form, MESMO has constant NO_3 inventory (i.e., without denitrification and nitrogen fixation). However, A. Ridgwell has already coded denitrification in BIOGEM and we in Minnesota have coded a simple nitrogen fixation scheme according to the distribution of $N*$ (Gruber and Sarmiento, 1997), a quasi-conservative tracer used to infer the regions of nitrogen fixation. Our diagnostic scheme adds NO_3 lost by denitrification back to the system to preserve the initial oceanic inventory. We have also developed the ^{15}N isotope to accompany these processes. However, these N-cycle processes are not activated at this time in MESMO, as they would require significant calibration effort, which we will expend in the future when they become necessary to address the question at hand.

Equation (4) also includes aqueous CO_2 as a nutrient, so that we may examine possible fertilization effects due to

Table 2. Comparisons of key physical model diagnostics.

Metrics	Targets	GENIE-1	G1-16lev	Control	K_v_prof	FWFlux	Season	ATMdif	Drake	MESMO
$\Delta^{14}C$ (‰)										
NADW	-67 ± 29[a]	-53	-84	-76	-112	-75	-77	-75	-76	-99
CDW	-155 ± 12[a]	-82	-123	-99	-164	-100	-99	-104	-99	-153
NPDW	-226 ± 14[a]	-140	-188	-142	-223	-144	-139	-145	-141	-216
MOC (Sv)										
Atlantic	14–27[b]	16	16	16	9	19	14	17	17	12
Southern Ocean	18–30[b]	36	22	13	25	12	15	10	19	25
Temperature r^2										
Surface (0–45 m)		0.90	0.95	0.96	0.95	0.96	0.96	0.95	0.96	0.95
Global		0.91	0.93	0.94	0.93	0.94	0.94	0.93	0.94	0.92
Salinity r^2										
Surface (0–45 m)		0.39	0.43	0.53	0.43	0.49	0.53	0.53	0.53	0.44
Global		0.47	0.54	0.59	0.54	0.53	0.55	0.58	0.59	0.45
1994 inventories										
CFC-11 (mol$\times10^6$)	0.55 ± 0.12[c]	0.92	0.91	1.10	0.68	1.06	1.10	0.99	1.10	0.69
Anthropogenic CO_2 (PgC)	118 ± 19[d]	171	154	176	120	169	179	168	179	118

[a] Matsumoto et al. (2004)
[b] Doney et al. (2004)
[c] Willey et al. (2004)
[d] Sabine et al. (2004)

increasing atmospheric CO_2 content in the future. Under optimal light and nutrient conditions, $CO_2(aq)$ can limit the photosynthetic rate even with abundant DIC, if the diffusive CO_2 transport is sufficiently slow (Riebesell et al., 1993).

The light or solar irradiance limitation is given by:

$$F_I = \frac{I}{I + K_I}, \quad (5)$$

where I is the seasonally variable solar short-wave irradiance, which decays exponentially from the ocean surface with a 20 m depth scale, and K_I (20 W/m^2) is the light limitation term (Doney et al., 2006).

The proxy for biomass B (μmol/L) is the concentration of the limiting nutrient, determined in Eq. (4). The basic idea, following Doney et al. (2006), is that the higher the concentration of the limiting nutrient, the larger the phytoplankton biomass or population that can be supported.

Second, remineralization of labile particulate organic matter (POM) in MESMO is now expressed by its sinking rate and temperature dependent remineralization rate (Matsumoto, 2007). This is a more process oriented representation over the original expression in GENIE-1 that uses a predefined remineralization profile like the so-called 'Martin curve' (Martin et al., 1987). The sinking rate in our formulation is a parameter to be determined by calibration. The temperature dependent remineralization rate follows the $Q_{10}=2$ relationship. It allows for a climate-carbon cycle feedback, which in the context of glacial-interglacial cycles can be important (Matsumoto, 2007).

Third, the artificial limitation on air-sea gas exchange that Ridgwell et al. (2007) employed to achieve numerical stability (existed in CB-GOLDSTEIN Version 6 but not described in the literature) has been removed. The gas exchange coefficient in GENIE-1 was based on the work of Wanninkhof (1992). We retained the Wanninkhof coefficient, because it remains the de facto standard in existing ocean carbon cycle models. However, a recent reanalysis of bomb ^{14}C inventory in the ocean, which constrains the global gas exchange coefficient, suggests that the Wanninkhof rate may be too high (Sweeney et al., 2007). As shown by Sarmiento et al. (1992), gas exchange would have a more significant impact on "slow" equilibration gases such as $^{14}CO_2$ than on "fast" gases such as CO_2 and CFCs, a result we confirmed with MESMO. Therefore, if a reduction in the global gas exchange is truly in order, our choice of the Wanninkhof coefficient would tend to overestimate the deep ocean ^{14}C abundance with minimal effect on anthropogenic CO_2 and CFCs.

4.3 Attempted but ultimately discarded improvements to MESMO

Briefly we note two attempts to improve the physical climate model that in the end we did not adopt: deepening the Drake Passage and reducing the diffusivity of heat in the atmosphere at 60° S. Results are shown in Table 2 as Experiments Drake and ATMdiff. Both features were suggested as possibly helpful in improving the deep ocean ventilation by T. Lenton and R. Marsh in their experiences with GENIE-1. The Drake Passage deepening has the potential
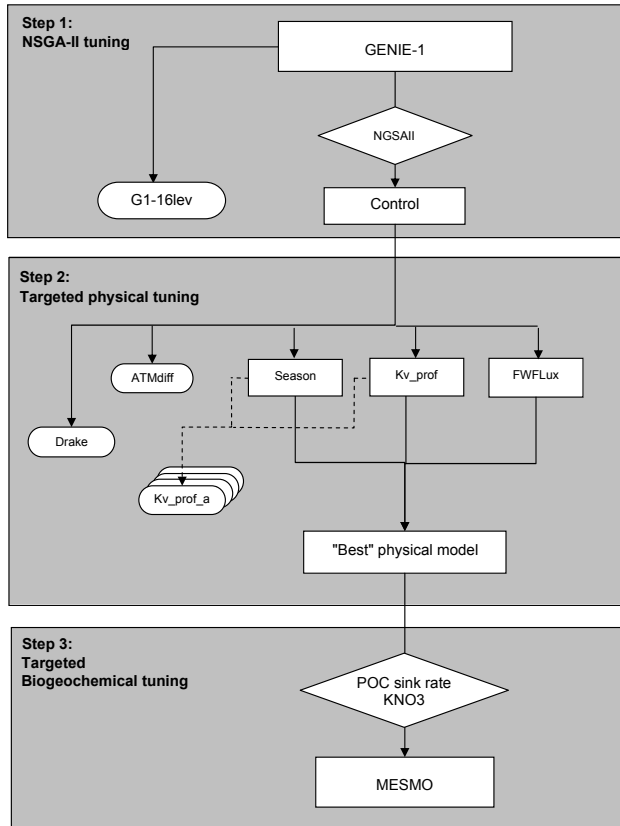
Fig. 1. Flow chart for the entire MESMO calibration process that includes three steps: (1) NGSA-II objective optimization; (2) targeted physical tuning; (3) targeted biogeochemical tuning. See text for details.

Fig. 2. Flow chart for the NSGA-II with surrogate modeling optimization process.

to homogenize the Deep South Atlantic and South Pacific by allowing a larger transport of Antarctic Circumpolar Current (ACC) through the passage. Reduced atmospheric diffusivities have the effect of thermally isolating Antarctica from the rest of the globe and thereby cooling and forming Antarctic Bottom Water (AABW). As shown in Table 2, we found that these did not significantly improve MESMO beyond the large improvements gained by our depth dependent K_v profile. This combined with the rather ad hoc nature of the improvements lead us to not implement these into MESMO.

5 Calibration and control run of MESMO

The equilibrium runs for all our model configurations are obtained by running the model many thousand years until steady state is reached. Metrics used to evaluate the equilibrium runs are the distributions of temperature and salinity, Atlantic MOC, and Southern Ocean MOC (Table 2). The postindustrial transient run is obtained by running the model from the preindustrial state, taken to be year 1765 and represented by the equilibrium run, to the year 1994 following the
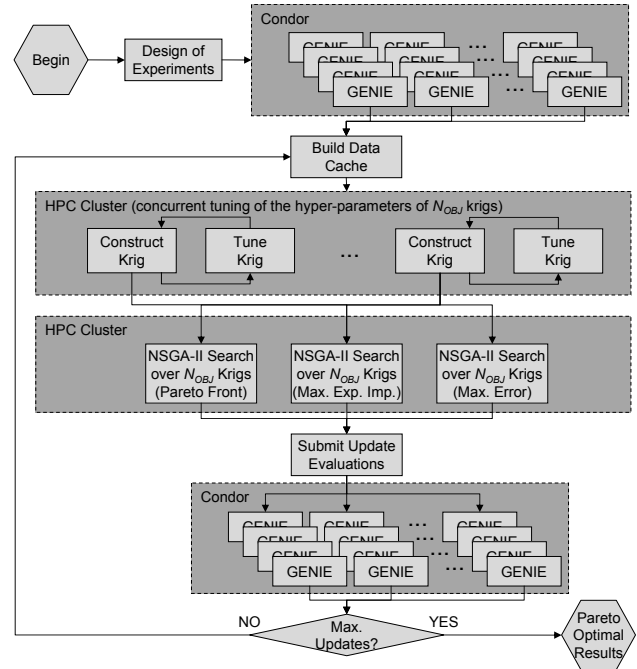
OCMIP-2 HISTORICAL protocol. In the protocol, the physical model state remains unchanged (i.e., without radiative feedback), while the atmospheric CFC-11 and pCO_2 concentrations are prescribed to follow observations, so that the total oceanic uptake of CFC-11 and anthropogenic CO_2 can be modeled and compared to data-derived estimates for the year 1994 (Table 2). These are also diagnostic of the physical model, because their oceanic uptake is determined to first order by abiotic processes (solubility and vertical mixing).

First, we consider what would happen if we were to just take the GENIE-1's 8-level model parameter values and use them in the new 16-level configuration (Experiment G1-16lev, Table 2). Compared to GENIE-1, G1-16lev equilibrium run shows some improvement with older Δ^{14}C everywhere in the deep ocean as a result of reduced Southern Ocean MOC. However, the mismatch relative to observations is still significant (deep Pacific still about 50% too young). There is also minor improvement in matching the observed temperatures and salinities as well as CFC-11 and anthropogenic carbon inventories.

The improvements realized in G1-16lev over GENIE-1 are insufficient (Table 2) so that a more thorough tuning process for MESMO is needed. Our strategy is to do it in three steps (Fig. 1). First, we calibrate the physical model by an objective tuning procedure NGSA-II that only uses the physical climatology fields as targets (Sect. 5.1.1). Second, we employ a subjective, target tuning to further improve the physical model (Sect. 5.1.2). Third, we take the best physical

model from the first two steps and tune the biogeochemistry model by seeking to minimize errors in two model outputs, export production and interior oxygen distribution (Sect. 5.2).

A number of factors lead to the adoption of this three-step tuning procedure. A lesson from OCMIP-2 was that the uptake of anthropogenic transient tracers is quite variable in different ocean carbon cycle models because their physics, defined in the broadest sense (e.g., resolution, forcings, numerics, sea ice, seasonality, GM), was so diverse (Doney et al., 2004; Dutay et al., 2002; Matsumoto et al., 2004). OCMIP-2 showed that biogeochemical tracers are very effective in evaluating the ventilation rate of the ocean interior, because the tracers have built-in clocks. So they must be part of our metrics. While it is more preferable to include biogeochemical tracers as targets in the objective tuning (i.e., combine steps one and two), we were guided on practical grounds to keep the first two steps separated because objective tuning using only physical climatology fields exists already in the form of NGSA-II. Earlier tuning studies of GENIE-1 also used only physical fields (Edwards and Marsh, 2005; Lenten et al., 2006). We are also guided by the expectation that objective tuning will likely not give us the most desirable model configuration outright and that some form of subjective tuning based on expert judgment is necessary. The limitations of objective tuning in GENIE-1 is evident, for example, in Lenten et al. (2006) who demonstrated that hand-tuning can do better than objective tuning. Also, in their first objective optimization of C-GOLDSTEIN, Edwards and Marsh (2005) found that the acceptable range of parameter values after optimization remained as large as the range across the initial ensemble.

5.1 Physical model calibration

5.1.1 First step: multi-objective NSGA-II tuning

Our goal is to find a combination of physical model parameters that minimize the mismatch between model-simulated fields and equivalent observed fields. The observed fields are air temperature, air humidity, ocean temperature, and ocean salinity. The non-linear response of the model to its parameters and the possible conflicts between the objectives make this task a challenge. We apply a multi-objective optimization method, which uses a population based algorithm to seek pareto-optimal solutions in the parameter space. For each field i an objective measure of the model's mismatch to the observational data is evaluated at the end of a simulation as

$$f_i(x) = \sqrt{\frac{(s_i(x) - S_i)^2}{\hat{\sigma}_i^2}}, \tag{6}$$

where the squared difference between the model field s_i and equivalent observational data S_i is weighted by the variance in the observational data σ_i^2. The optimization process seeks to minimize the value of this function over each of the four

physical fields, producing a pareto-optimal set of parameter sets, the solutions that are better than all the rest in at least one of the objectives. A post-processing of the result set then yields an optimal version of the model. Previous parameter estimation techniques applied to the C-GOLDSTEIN class of problem include a Latin Hypercube sampling (Edwards and Marsh, 2005), the Ensemble Kalman Filter (Hargreaves et al., 2004), the proximal analytic centre cutting plane method (Beltran et al., 2005) and kriging (Price et al., 2007) which all seek to minimize a composite error function. The multi-objective method has the advantage that it avoids the need to select a priori the weighing factors used to evaluate the single error value.

For the purposes of the MESMO calibration, individual model runs were integrated over 5000 years to ensure the system reached quasi-equilibrium. With 16 vertical levels in the ocean, the typical execution time for a simulation was between 150 and 250 min CPU time on the range of compute resource available. This represents an increase in the CPU wall-time of a simulation by a factor of ~4 over the C-GOLDSTEIN model studied in previous exercises. A standard application of the NSGA-II algorithm (Deb et al., 2002) would therefore have required several weeks of compute time to achieve a high quality result. In order to reduce the required time, we employed the NSGA-II method with surrogate modeling. Previous work (Price et al., 2006) has shown that the use of surrogate models with the NSGA-II algorithm can reduce, by an order of magnitude, the total number of simulation years required for a high quality result in the calibration of the C-GOLDSTEIN composition.

The optimization process is illustrated in Fig. 2. The method consists of an initial sampling of the parameter space from which surrogate models of the underlying objective functions are built. These computationally cheap surrogate models are then searched extensively using the NSGA-II algorithm to generate a set of update points that are evaluated on the true objective functions. The algorithm iterates by refining the surrogate models and performing the NSGA-II search over the new models until convergence criteria are satisfied or available computational budget is exhausted. At the end of the process the pareto-optimal points in the objective space of the problem are returned for further analysis. The technical details of the optimization process are described as a supplemental material and in Price et al. (2006).

Figure 3 shows the results of the optimization process. A total of 137 members of the data cache comprise the Pareto front, indicated by red dots in the figure. Following Price et al. (2006) we use the C-GOLDSTEIN weighting of the objectives to evaluate a single error function value for each data point. The progress of the algorithm, as measured by this single error function, is shown in the bottom left plot. The composite function weights the objectives by the reciprocal of the variance in the observational data and by the number of grid cells in the field. Since the observational data has not changed, the only difference in this measure for MESMO
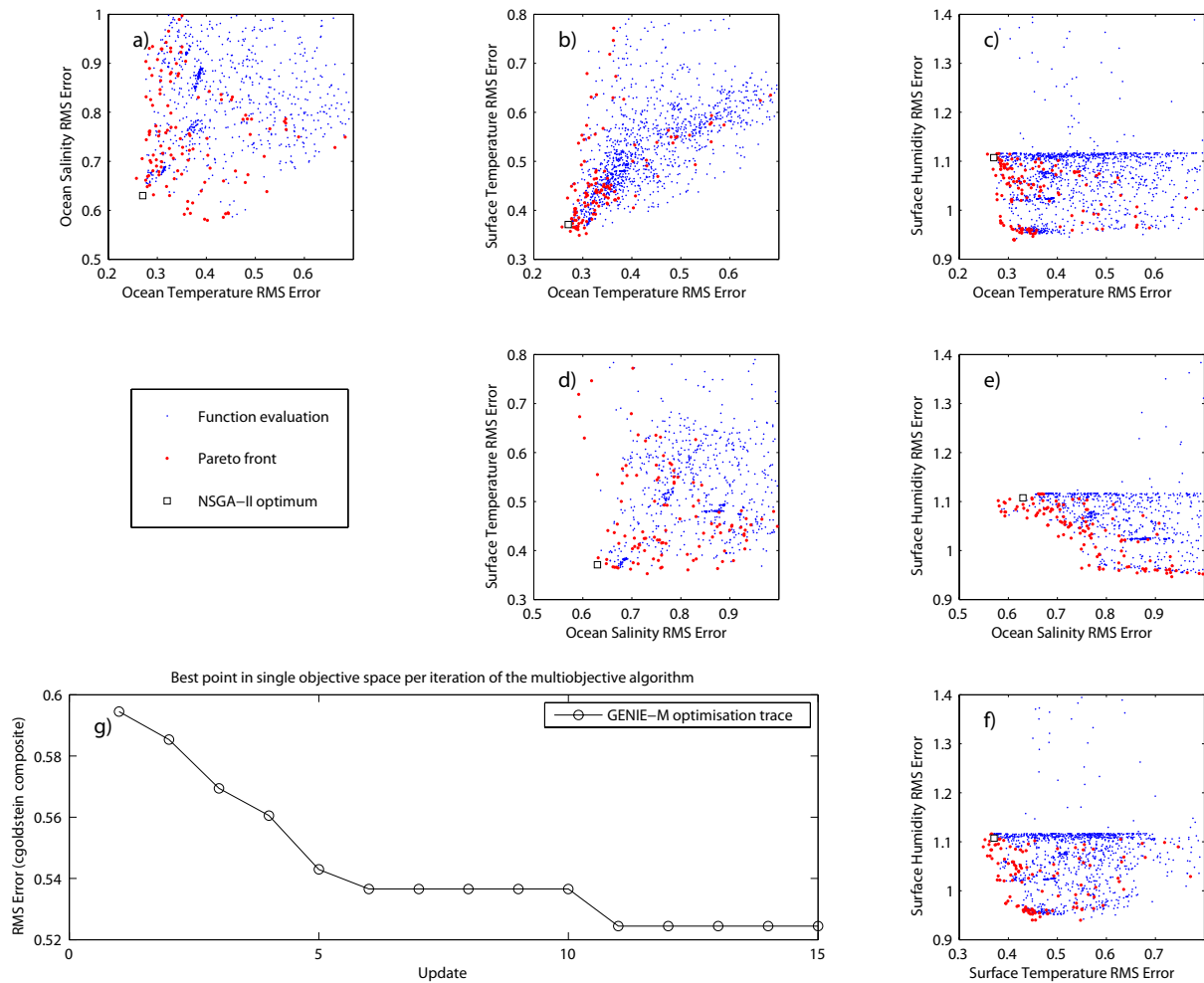
Fig. 3. Results of the NSGA-II optimization of the MESMO model plotted across each 2-D projection of the four objective functions **(a–f)** as calculated in Eq. (6) for the fields ocean temperature, ocean salinity, surface temperature and surface humidity. The red points indicate model evaluations that lie on the Pareto front and dominate the other evaluations marked with blue points. The progress of the algorithm is displayed in plot **(g)** as measured by the minimum of the weighted root mean square of the four objective values across all members in the data cache after each update.

over C-GOLDSTEIN comes from the increase in the number of grid cells upon doubling the vertical layers. It is therefore noted that the doubling of the ocean levels in this version of the model has increased the bias of this measure further towards the ocean fields. The optimal point we have selected therefore sits closest to the origin of the T vs. S plot and achieves the best ocean interior at the expense of a less optimal surface humidity representation.

The version of C-GOLDSTEIN that was optimized using NSGA-II was the original version of Edwards and Marsh (2005) modified to include our new 16 vertical levels and GM parameter ssmax. The twelve "best" model parameter values from NSGA-II are listed in Table 1. The model runs using the NSGA-II values constitute our Control experiment (Table 2). Compared to GENIE-1, the equilibrium Control run shows modest improvements in simulating the observed deep ocean

Δ^{14}C as well as ocean temperature and salinity distributions. The deep Δ^{14}C is still too young though, especially for the Circumpolar Deep Water (CDW, -99%) and the North Pacific Deep Water (NPDW, -142%) compared to observations (-155% and -226%, respectively). Improvement in matching the observed temperatures is quite modest, because SST and global ocean temperatures in GENIE-1 were already reasonably good (r^2 of 0.9 and higher). The Control run shows more improvement over GENIE-1 in ocean salinities, although r^2 for salinity is in general much lower than for temperature. However, we are dissatisfied with our transient Control run in that it overestimates the transient tracer uptake (1.10×10^9 mol CFC-11 and 176 Pg of anthropogenic carbon) even more than GENIE-1 (0.92×10^9 mol CFC-11 and 171 Pg-C) .

5.1.2 Second step: targeted tuning

Given our original motivation, MESMO must show improvements in transient tracer metrics in particular. We therefore build on NSGA-II tuning with three targeted tunings (K_v_prof, FWflux, and Season) aided by some knowledge from experience about how they will affect the results (Table 2).

The single most important change that improved the transient tracer uptake was K_v_prof. This alone brought the model-predicted transient tracer uptake very close to data-based estimates: CFC-11 inventory is 0.68×10^9 mol in the model compared to $0.55 \pm 0.12 \times 10^9$ mol based on data (Willey et al., 2004); anthropogenic carbon inventory is 120 Pg-C in the model compared to 118 ± 19 Pg-C based on data (Sabine et al., 2004). The reduced transient uptake is a direct consequence of the low K_v in the upper ocean in K_v_prof. It is an expected consequence, given that CFCs and CO_2 have relatively short timescale of air-sea gas equilibration, so their uptake is controlled predominantly by vertical exchange in the ocean rather than air-sea gas exchange kinetics. The reduced upper ocean K_v has the added and significant benefit of making the deep ocean older with respect to $\Delta^{14}C$. The ventilation of the deep Southern Ocean ($\Delta^{14}C = -164$‰) and Pacific Ocean ($\Delta^{14}C = -223$‰) are now consistent with observations (Table 2). One drawback in K_v_prof is reduced Atlantic MOC, which is now 9 Sv compared to 16 Sv in both GENIE-1 and the Control run (Table 2).

Equation (1) represents our choice of the K_v profile that is adopted in MESMO, but we have explored the effects of changing the shape of the profile (Fig. 4). We find that shoaling the inflection point (say, by 1000 m; compare profiles A and B which are otherwise identical) increases ventilation of CDW ($\Delta^{14}C = -148$‰ for A and -139‰ for B) and NPDW ($\Delta^{14}C = -200$‰ and -181‰), without little effect on the NADW (both $\Delta^{14}C = -109$‰). Likewise, the sharper transition from low to high values in profile C as compared to profile D yields older CDW $\Delta^{14}C$ (-173‰ for C and -167‰ for D) and NPDW (-233‰ for C and -224‰ for D); the sharper transition keeps K_v above the inflection point to a lower value, to which the deep ocean ventilation is sensitive. As noted above, our choice of the K_v profile was guided by observations (Ledwell et al., 1993; Ledwell et al., 1998), history (Bryan and Lewis, 1979), and NGSA-II results (Table 1).

In addition to K_v_prof, we made two modifications to arrive at our best model, which constitutes the physical model of MESMO. First, we implemented FWflux in order to restore the Atlantic MOC that was reduced to 9 Sv in K_v_prof. With FWflux, the Atlantic-to-Pacific freshwater flux is increased by 25% from the value given by NGSA-II (Table 1). As shown earlier for GENIE-1 (Marsh et al., 2004, 2007), this has the effect of increasing the Atlantic MOC by increasing salinity and thus density of the Atlantic surface waters. The interbasin water transport is an needed in GENIE-1 to
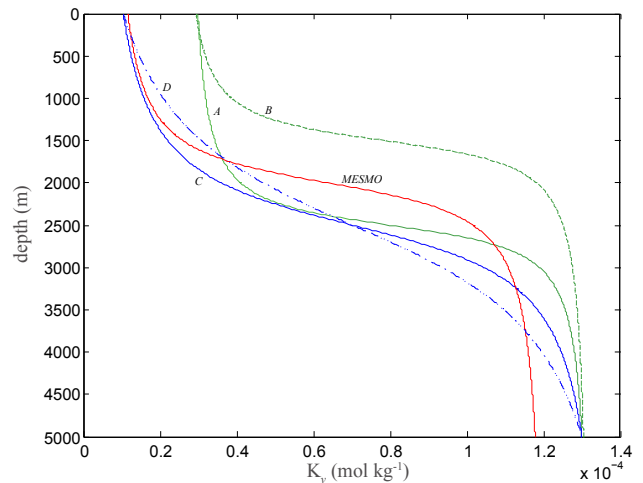

Fig. 4. Various depth profiles of vertical diffusivity K_v. MESMO profile (red solid line) represents Eq. (1). Profiles A (green solid) and B (green dashed) are identical except the depth of the arctangent inflection point is offset by 1000 m. Profiles C (blue solid) and D (blush dashed-dot) are identical except the rapidity of transition between the low K_v above the inflection point and the high K_v above is different.

compensate for the insufficient transport in the energy moisture balance model of the atmosphere (Edwards and Marsh, 2005). This is an artificial flux adjustment, which should ideally be gotten rid of. Our decision to increase it therefore represents a drawback in MESMO, as a larger adjustment helps achieve a better match with observations in the equilibrium at the likely expense of (weak) transient response.

Second, we implemented Season in order to simulate the seasonality and spatial coverage of sea ice (Fig. 5, see animation of seasonality in Supplemental Materials). In the Control and K_v_prof-only models, which lack seasonal variability in solar radiation, sea ice is largely permanent where it exists (i.e., 100% in Fig. 5a, c). With Season, polar sea ice extent is seasonal (Fig. 5b, d). In our best model (Fig. 5d), sea ice coverage around Antarctica is approximately 4.5×10^6 km^2 during summer and 36×10^6 km^2 during winter. These overestimate somewhat the satellite-derived sea ice climatology for the 1979–2000 period that shows summer coverage of 3–4×10^6 km^2 and winter coverage of 17–20×10^6 km^2 (National Snow and Ice Data Center, http://www.nsidc.colorado.edu). However, the percent change in sea ice coverage in the two seasons is comparable in MESMO and observations.

In our best physical model of MESMO (Table 2; salient features shown in Fig. 6), the benefits of K_v_prof in terms of deep ventilation (consistent in $\Delta^{14}C$) and transient tracer uptake (0.67×10^9 mol-CFC-11 and 118 Pg-C) are still preserved. The Atlantic MOC is reasonable, again at the expense of a larger flux adjustment, and a more realistic seasonality of polar sea ice is achieved.
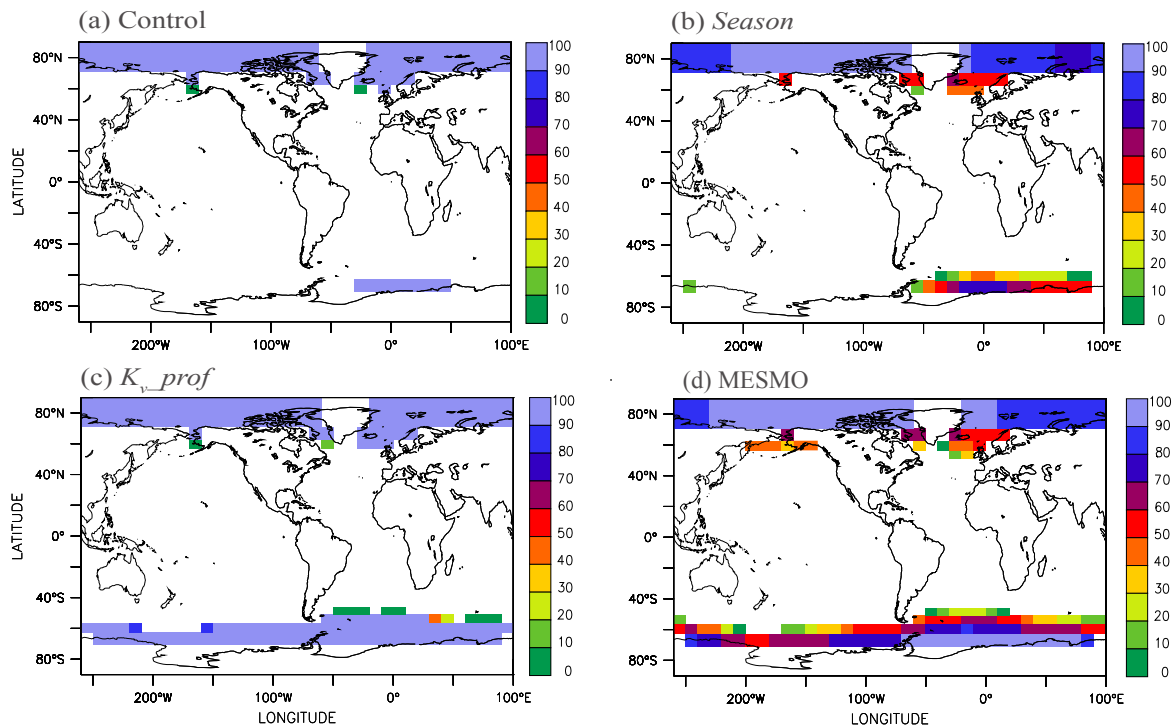
Fig. 5. Sea ice coverage from equilibrium runs of **(a)** Control, **(b)** Season, **(c)** K_v_prof, and **(d)** MESMO. Percentage of sea ice coverage at each grid point over a course of one year is shown. So a 50% coverage may be due to: 100% coverage for half a year, 50% coverage for all year, or some intermediate combination between the two extreme cases. See Supplemental Materials for animation of the seasonal cycle.

5.2 Biogeochemistry model calibration

We now calibrate our best physical model in terms of biogeochemistry using two targets, global particulate organic carbon (POC) export and the global ocean distribution of dissolved oxygen (O_2). Both are representative of marine biogeochemistry and important diagnostics of vertical nutrient supply and remineralization (Gnanadesikan et al., 2004). We also used NO_3 and ALK as targets but these are not as sensitive to change and therefore of secondary importance to POC export and O_2.

Model parameters to be determined are the half saturation constants in Eq. (4) and the sinking rate of POC. This is done by sweeping a parameter space defined by these parameters and seeking a combination of parameters that best reproduces the observed POC export and O_2. We start by assuming that K_{NO_3} and K_{PO_4} are simply related by a stoichiometry of 16. This makes NO_3 rather than PO_4 the more important limiting nutrient, but otherwise, the two macronutrients are qualitatively very similar in behavior at this time. In the future, when iron, nitrogen fixation, and denitrification become operational, NO_3 and PO_4 will become more meaningful as independent nutrient tracers. As for $K_{CO_2(aq)}$, we use the value of 0.5×10^{-6} mol kg^{-1} (Riebesell et al., 1993) and keep it constant, since little is actually known about CO_2 limitation and much of what is known comes from the work of Riebesell.

Our parameter space is therefore defined by K_{NO_3} and the POC sink rate (Fig. 7). For the chosen ranges of these parameters, our model gives global POC export production between 6 and 11 Pg-C yr^{-1} (Fig. 7a). The range in data-based estimates using satellite products and inverse modeling is roughly 9 to 13 Pg-C yr^{-1} (Gnanadesikan et al., 2004; Laws et al., 2000; Schlitzer, 2002) with possibly significant uncertainties (Najjar et al., 2007). In our model, export production is sensitive to POC sinking rate within the parameter space, and it indicates that our sinking rate should be in the lower range to be consistent with data-based estimates.

Comparison of the global O_2 distribution between our model and observations (Levitus and Boyer, 1994a) indicates that spatial correlation is also higher for lower POC sinking rates (Fig. 7b). The r^2 value for the global ocean reaches as high as 0.7 for sinking rate of 50 m day^{-1}.

A closer look at the absolute value of dissolved O_2 in the upper ocean and deep ocean indicates that the choice of K_{NO_3} is also important (Fig. 8). Above water depths of 1500 m (Fig. 8a), deviation from observations becomes as small as 5 μmol kg^{-1} when K_{NO_3} is about 0.3×10^{-5} mol kg^{-1}. Larger K_{NO_3} gives larger errors, as large as 30 μmol kg^{-1}. Below 1500 m (Fig. 8b), O_2 becomes significantly depleted with higher POC sinking rate and consequently more POC being remineralized in the deeper waters.

Given these constraints, we chose POC sinking rate of 50 m day^{-1} and K_{NO_3} of 0.34×10^{-5} mol kg^{-1} for MESMO.
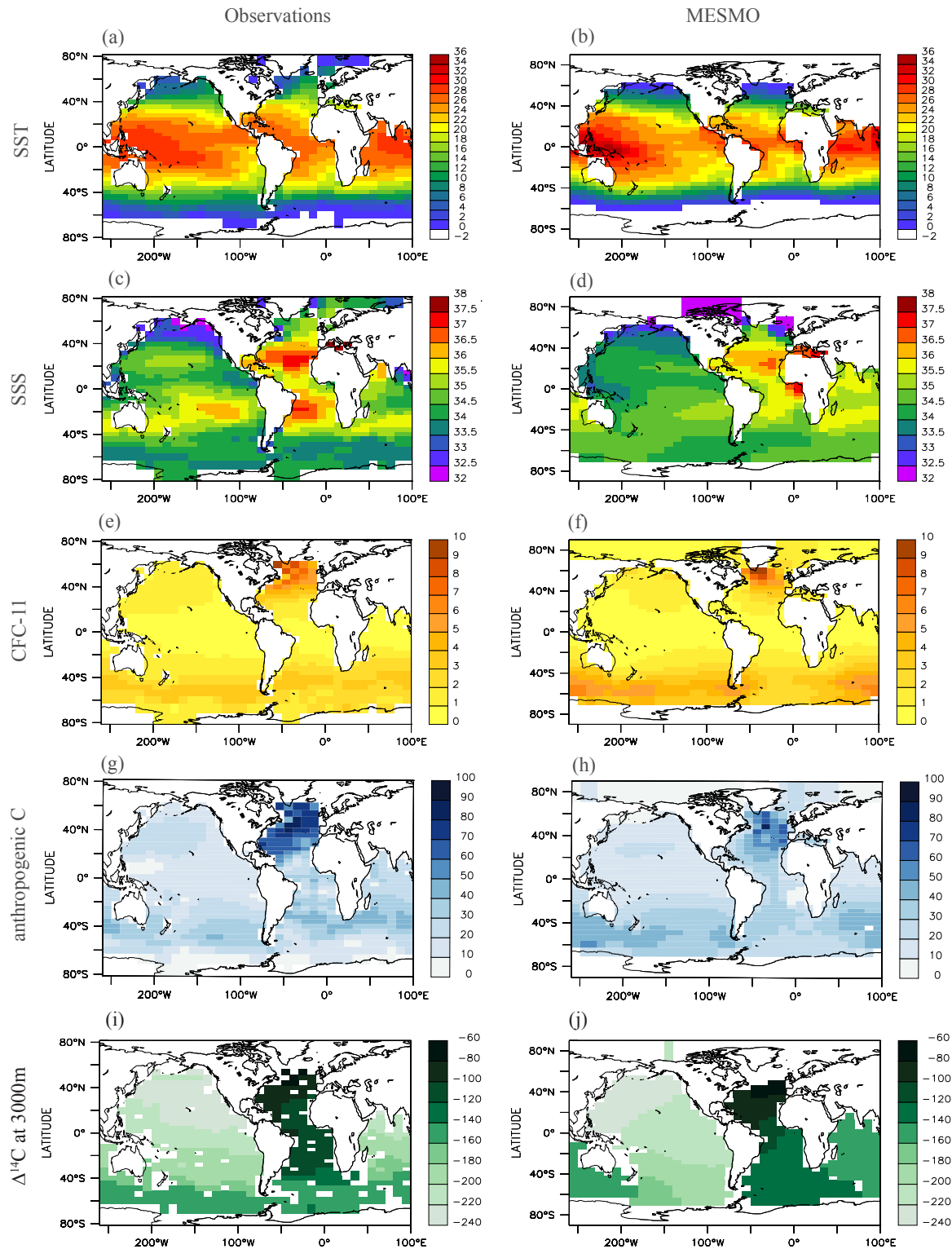
Fig. 6. Key diagnostics of MESMO (right column) compared to equivalent "observations (left column). Annually averaged sea surface temperatures **(a, b)** and salinities **(c, d)**. 1994 column inventories of CFC-11 in mole m^{-2} **(e, f)** and anthropogenic carbon in mole m^{-2} **(g, h)**. Natural Δ^{14}C at 3000 m in ‰ **(i, j)**. Gridded observations and data-derived estimates (Key et al., 2004; Levitus and Boyer, 1994a, b; Sabine et al., 2004; Willey et al., 2004) were regridded to the MESMO grid using the built-in regridding transformations in Ferret distributed by PMEL/NOAA (http://ferret.pmel.noaa.gov/Ferret/home).

(a) Global POC export

(b) Global O$_2$ r^2
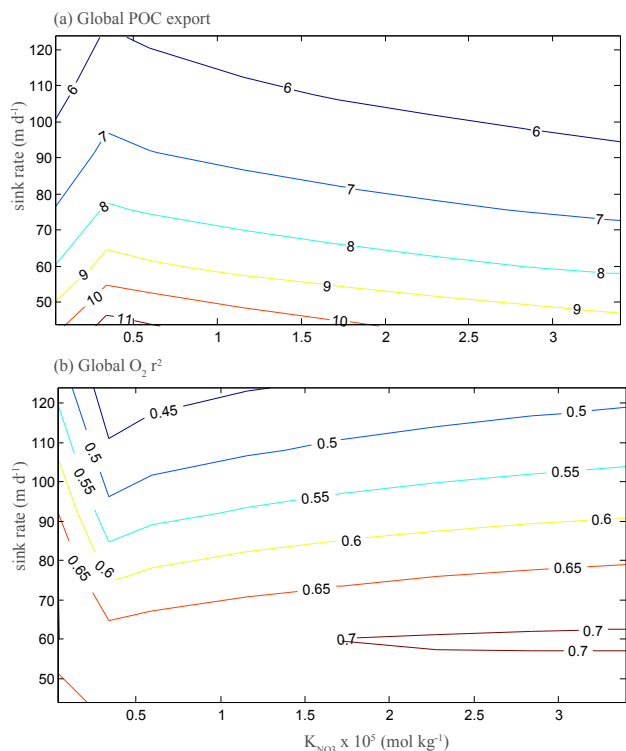
Fig. 7. Global POC export and model-data dissolved O$_2$ correlation in a parameter space defined by POC sinking rate and K$_{NO_3}$. For POC export **(a)**, date based estimates range from 9 to 13 Pg-C yr^{-1}. For dissolve O$_2$ correlation **(b)**, we seek the highest correlation. Units are Pg-C yr^{-1} for POC export and r^2 value for O$_2$ correlation.

Export POC (see animation of seasonality in supplemental materials: http://www.geosci-model-dev.net/1/1/2008/gmd-1-1-2008-supplement.zip) and CaCO$_3$ production in MESMO are respectively 10.6 Pg-C yr^{-1} and 0.9 Pg-C yr^{-1} compared to 8.9 Pg-C yr^{-1} and 1.2 Pg-C yr^{-1} in GENIE-1. The r^2 value for the global O$_2$ distribution between model and data is 0.70 in MESMO compared to 0.56 in GENIE-1. In MESMO, the total inventory of DIC is 36.737 Pg-C and of ALK is 3.2×10^{18} mole-eq.

6 Discussion and summary

Significant improvements are achieved in MESMO over its predecessor GENIE-1. Whereas GENIE-1 had excessive ventilation (Δ^{14}C was too high in all basins, global CFC inventory was almost twice the observation, and anthropogenic carbon inventory was about 50 Pg-C too large), MESMO is consistent with all these data-based metrics (Table 2). Export POC production in MESMO is 10.6 Pg-C yr^{-1}, which is in good agreement with the data-based estimates. Dissolved O$_2$ in the ocean interior is modestly improved in MESMO over GENIE-1 in terms of model-data correlation. The improvements in interior ventilation rates as indicated by Δ^{14}C
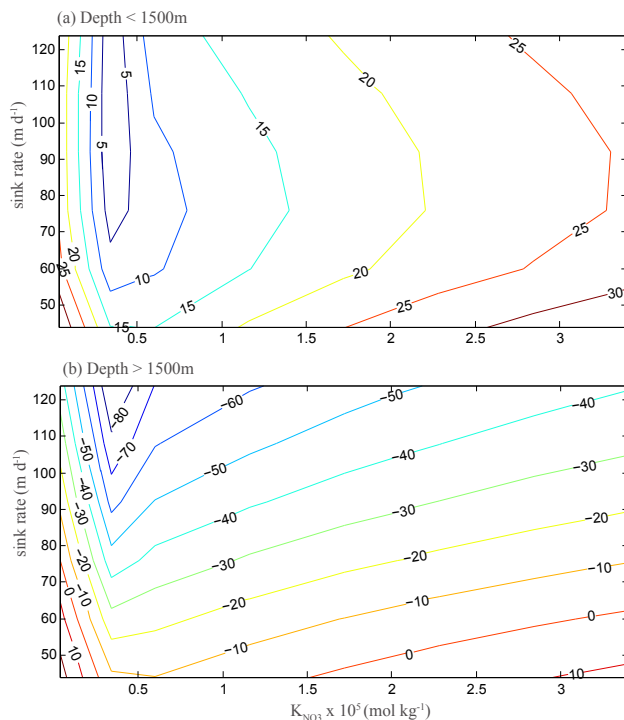
(a) Depth < 1500m

(b) Depth > 1500m

Fig. 8. Model-data difference in dissolved O$_2$ **(a)** above 1500 m water depth and **(b)** below 1500 m in μmol kg^{-1}. We seek the smallest error from observations in both.

and dissolved O$_2$ are not unrelated, because the latter reflects a balance between the rate of ventilation that supplies O$_2$ to the interior and the production of POC that ultimately depletes O$_2$.

These improvements were achieved while increasing the vertical resolution of the upper ocean, which has important implications. Again, the thickness of the topmost ocean layer is 45 m in MESMO compared to 175 m in GENIE-1. In MESMO, production occurs in the top two layers in 100 m and is modified by diagnosed mixed layer depth (Fig. 9a, see animation of seasonality in Supplemental Materials). The physical setting that defines production is thus better represented in MESMO. The reduced thickness of the topmost layer is also important in setting the right physical conditions for air-sea gas exchange. Tracers such as CFC-11 have relatively short gas equilibration time scale and surface waters are fairly close to being saturated, especially away from the polar sea ice. It is desirable for the CFC-saturated, topmost layer, to be appropriately thin in order to get the tracer inventory correct for the right reason.

In calibrating MESMO, we used the results of NGSA-II as starting point, from which significant improvements were made by targeted tuning based on experience. The most important targeted, physical tuning was the depth dependent vertical mixing K_v_prof, followed by Season to achieve a better seasonal variability of polar sea ice, and FWflux, to
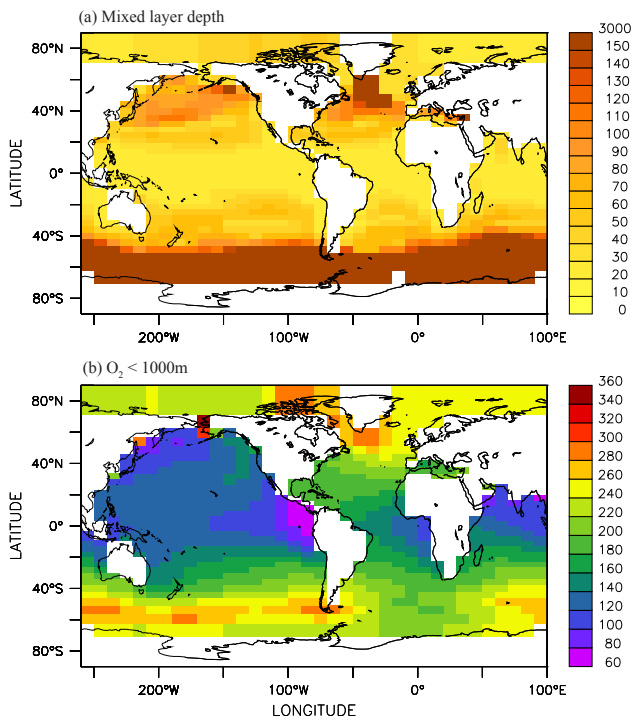
Fig. 9. MESMO results: **(a)** annually averaged, diagnosed mixed layer depth in meters and **(b)** dissolved O_2 in the upper 1000 m. See Supplemental Materials for animation of the mixed layer depth.

maintain an adequate vigor in the Atlantic MOC. In biogeochemistry calibration, we defined a parameter space defined by two key parameters, and chose a combination of these parameters that minimized the error in reproducing the dissolved O_2 distribution and global POC production.

We believe that MESMO, with significant improvements over its predecessor, makes it a well calibrated EMIC for studies of the global carbon cycle of both today and the recent past. The improved physical setting for surface production makes it suitable to examine the feedbacks of marine biology to climate change, although the larger freshwater flux adjustment in MESMO may reduce the sensitivity of the Atlantic MOC to certain perturbations.

We expect to further develop MESMO in the future. There are two specific improvements on the horizon. First, incorporation of iron would likely help improve the spatial distribution of export production and thus interior O_2 distribution. For example, Fig. 9b shows that the upper ocean of the eastern equatorial Pacific is low in O_2 as we expect but not low enough to initiate denitrification as observed. An accurate representation of the dissolved O_2 is critical for a reasonable marine nitrogen cycle, which in turn allows nitrogen and phosphate cycles to become decoupled. This would allow NO_3 and PO_4 along with iron to be meaningful limiting nutrients in MESMO. Second, forcing MESMO with seasonal wind stresses will make it a more truly dynamically seasonal model. We have in fact begun to do this with the ECMWF seasonal wind stress fields , although preliminary efforts have produced too much interior ventilation, indicated by deep radiocarbon and transient tracer uptake, and too much export production.

Edited by: A. Ridgwell

References

Bryan, K. and Lewis, L. J.: A water mass model of the world ocean, J. Geophys. Res., 84, 2503–2518, 1979.

Chikamoto, M. O., Matsumoto, K., and Ridgwell, A.: Response of deep-sea $CaCO_3$ sedimentation to Atlantic meridional overturning circulation shutdown, J. Geophys. Res., doi:10.1029/2007JG000669, in press, 2008.

Claussen, M., Mysak, L. A., Weaver, A., Crucifix, M., Fichefet, T., Loutre, M. F., Weber, S. L., Alcamo, J., Alexeev, V., Berger, A., Calov, R., Ganopolski, A., Goosse, H., Lohmann, G., Lunkeit, F., Mokhov, I. I., Petoukhov, V., Stone, P. and Wang, Z.: Earth system models of intermediate complexity: Closing the gap in the spectrum of climate system models, Clim. Dynam., 18, 579–586, 2002.

Doney, D. C., Lindsay, K., Fung, I., and Jasmin, J.: Natural variability in a stable, 1000-year global coupled climate-carbon cycle simulation, J. Climate, 19(13), 3033–3054, 2006.

Doney, S. C., Lindsay, K., Caldeira, K., Campin, J.-M., Drange, H., Dutay, J.-C., Follows, M., Gao, Y., Gnanadesikan, A., Gruber, N., Ishida, A., Joos, F., Madec, G., Maier-Reimer, E., Marshall, J. C., Matear, R. J., Monfray, P., Najjar, R., Orr, J. C., Plattner, G.-K., Sarmiento, J., Schlitzer, R., Slater, R., Swathi, P. S., Totterdell, I. J., Weirig, M.-F., Yamanaka, Y., and Yool, A.: Evaluating global ocean carbon models: The importance of realistic physics, Global Biogeoch. Cy., 18, GB3017, doi:10.1029/2003GB002150, 2004.

Duffy, P. B., Caldeira, K., Selvaggi, J., and Hoffert, M. I.: Effects of subgrid-scale mixing parameterizations on simulated distributions of natural 14C, temperature and salinity in a three-dimensional ocean general circulation model, J. Phys. Oceanogr., 27, 498–523, 1997.

Dutay, J.-C., Bullister, J. L., Doney, S. C., Orr, J. C., Najjar, R., Caldeira, K., Campin, J.-M., Drange, H., Follows, M., Gao, Y., Gruber, N., Hecht, M. W., Ishida, A., Joos, F., Lindsay, K., Madec, G., Maier-Reimer, E., Marshall, J. C., Matear, R. J., Monfray, P., Plattner, G.-K., Sarmiento, J., Schlitzer, R., Slater,

R., Totterdell, I. J., Weirig, M.-F., Yamanaka, Y., and Yool, A.: Evaluation of ocean model ventilation with CFC-11: Comparison of 13 global ocean models, Ocean Model., 4, 89–120, 2002.

Edwards, N. R. and Marsh, R.: Uncertainties due to transport-parameter sensitivity in an efficient 3-D ocean-climate model, Clim. Dynam., 24, 415–433, 2005.

Edwards, N. R., Willmott, A. J., and Killworth, P. D.: On the role of topography and wind stress on the stability of the thermohaline circulation, J. Phys. Oceanogr., 28, 756–778, 1998.

England, M. H. and Rahmstorf, S.: Sensitivity of ventilation rates and radiocarbon uptake to subgrid-scale mixing in ocean models, J. Phys. Oceanogr., 29, 2802–2827, 1999.

Gnanadesikan, A., Dunne, J. P., Key, R. M., Matsumoto, K., Sarmiento, J. L., Slater, R. D., and Swathi, P. S.: Oceanic ventilation and biogeochemical cycling: Understanding the physical mechanisms that produce realistic distributions of tracers and productivity, Global Biogeochem. Cy., 18, GB4010, doi:10.1029/2003GB002097, 2004.

Griffies, S. M.: The Gent-McWilliams skew flux, J. Phys. Oceanogr., 28(5), 831–841, 1998.

Griffies, S. M., Harrison, M. J., Pacanowski, R., and Rosati, A.: A technical guide to MOM4, in: GFDL ocean group technical report No. 5, NOAA/Geophysical Fluid Dynamics Laboratory, 2004.

Gruber, N. and Sarmiento, J. L.: Global patterns of marine nitrogen fixation and denitrification, Global Biogeochem. Cy., 11, 235–266, 1997.

Houghton, J. T., Ding, Y., Griggs, D. J., Noguer, M., van der Linden, P. J., and Xiaosu, D.: Climate Change 2001 – The Scientific Basis: Contribution of Working Group I to the Third Assessment Report of the Intergovernmental Panel on Climate Change, Cambridge University Press, Cambridge, 944 pp., 2001.

IPCC: Climate Change 2007: The Physical Science Basis, Contribution of Working Group I to the Fourth Assessment Report of the Intergovernmental Panel on Climate Change, Cambridge University Press, Cambridge, 996 pp., 2007.

Key, R., Kozyr, A., Sabine, C., Lee, K., Wannikhof, R., Bullister, J. L., Feeley, R. A., Millero, F., Mordy, C., and Peng, T.-H.: A global ocean carbon climatology: Results from GLODAP, Global Biogeochem. Cy., 18, GB4031, doi:10.1029/2004GB002247, 2004.

Laws, E. A., Falkowski, P. G., Smith, W. O. J., Ducklow, H., and McCarthy, J. J.: Temperature effects on export production in the open ocean, Global Biogeochem. Cy., 14, 1231–1246, 2000.

Ledwell, J. R., Montgomery, E. T., Polzin, K. L., St. Laurent, L. C., Schmitt, R. W., and Toole, J.: Evidence for enhanced mixing over rough topography in the abyssal ocean, Nature, 403, 179–182, 2000.

Ledwell, J. R., Watson, A. J., and Law, C. S.: Evidence for slow mixing across the pycnocline from an open-ocean tracer-release experiment, Nature, 364, 701–703, 1993.

Ledwell, J. R., Watson, A. J., and Law, C. S.: Mixing of a tracer in the pycnocline, J. Geophys. Res., 103, 21 499–21 529, 1998.

Lenton, T. M., Marsh, R., Price, A. R., Lunt, D. J., Aksenov, Y., Annan, J. D., Cooper-Chadwick, T., Cox, J. D., Edwards, N. R., Goswami, S., Hargreaves, J. C., Harris, P. P., Jiao, Z., Livina, V. N., Payne, A. J., Rutte, I. C., Shepherd, J. G., Valdes, P. J., Williams, G., Williamsson, M. S., and Yool, A.: Effects of atmospheric dynamics and ocean resolution on bi-stability of

the thermohaline circulation examined using the Grid ENabled Integrated Earth system modelling (GENIE) framework, Clim. Dynam., 29, 591–613, doi:10.1007/s00382-007-0254-9, 2007.

Lenton, T. M., Williamson, M. S., Edwards, N. R., Marsh, R., Price, A. R., Ridgwell, A., Shepherd, J. G., and The Genie team: Millenial timescale carbon cycle and climate change in an efficient Earth system model, Clim. Dynam., 26(7–8), 687–711, doi:10.1007/s00382-006-0109-9, 2006.

Levitus, S.: Climatological atlas of the world ocean, National Oceanic and Atmos. Admin., Rockville, Md., 1982.

Levitus, S. and Boyer, T. P.: World ocean atlas 1994, Vol. 2, Oxygen, National Oceanic and Atmospheric Administration, Washington, 186 pp., 1994a.

Levitus, S. and Boyer, T. P.: World ocean atlas 1994, Vol. 4, Temperature, National Oceanic and Atmospheric Administration, Washington, 117 pp., 1994b.

Maier-Reimer, E.: Geochemical cycles in an ocean general circulation model. Preindustrial tracer distributions, Global Biogeochem. Cy., 7(3), 645–677, 1993.

Marsh, R., Hazeleger, W., Yool, A., and Rohling, E. J.: Stability of the thermohaline circulation under millenial CO_2 forcing and two alternative controls on Atlantic salinity, Geophys. Res. Lett., 34, L03605, doi:10.1029/2006GL027815, 2007.

Marsh, R., Yool, A., Lenton, T. M., Gulamali, M. Y., Edwards, N. R., Shepherd, J. G., Krznaric, M., Newhouse, S., and Cox, S. J.: Bistability of the thermohaline circulation identified through comprehensive 2-parameter sweeps of an efficient climate model, Clim. Dynam., 23, 761–777, 2004.

Martin, J. H., Knauer, G. A., Karl, D. M., and Broenkow, W. W.: VERTEX: Carbon cycling in the northeast Pacific, Deep Sea Res., 34, 267–285, 1987.

Matsumoto, K.: Biology-mediated temperature control on atmospheric pCO_2 and ocean biogeochemistry, Geophys. Res. Lett., 34, L20605, doi:10.1029/2007GL031301, 2007.

Matsumoto, K. and Gruber, N.: How accurate is the estimation of anthropogenic carbon in the ocean? An evaluation of the ΔC^* method, Global Biogeochem. Cy., 19, GB3014, doi:10.1029/2004GB002397, 2005.

Matsumoto, K., Sarmiento, J. L., Key, R. M., Aumont, O., Bullister, J. L., Caldeira, K., Campin, J.-M., Doney, S. C., Drange, H., Dutay, J.-C., Follows, M., Gao, Y., Gnanadesikan, A., Gruber, N., Ishida, A., Joos, F., Lindsay, K., Maier-Reimer, E., Marshall, J. C., Matear, R. J., Monfray, P., Mouchet, A., Najjar, R., Plattner, G.-K., Schlitzer, R., Slater, R., Swathi, P. S., Totterdell, I. J., Weirig, M.-F., Yamanaka, Y., Yool, A., and Orr, J. C.: Evaluation of ocean carbon cycle models with data-based metrics, Geophys. Res. Lett., 31, L07303, doi:10.1029/2003GL018970, 2004.

Muller, S. A., Joos, F., Edwards, N. R., and Stocker, T.: Water mass distribution and ventilation time scales in cost-efficient, 3-dimensional ocean model, J. Climate, 19, 5479–5499, 2006.

Najjar, R. G., Jin, X., Louanchi, F., Aumont, O., Caldeira, K., Doney, S. C., Dutay, J.-C., Follows, M., Gruber, N., Joos, F., Lindsay, K., Maier-Reimer, E., Matear, R. J., Matsumoto, K., Monfray, P., Mouchet, A., Orr, J. C., Plattner, G. K., Sarmiento, J. L., Schlitzer, R., Weirig, M. F., Yamanaka, Y., and Yool, A.: Impact of circulation on export production, dissolved organic matter and dissolved oxygen in the ocean: Results from OCMIP-2, Global Biogeochem. Cy., 21, GB3007, doi:10.1029/2006GB002857, 2007.

Najjar, R. G. and Orr, J. C.: Biotic-HOW TO, Internal OCMIP Report, LSCE/CEA Saclay, Gif-sur-Yvette, France, 15 pp., 1999.

Pacanowski, R. C. and Griffies, S. M.: The MOM3 Manual, Alpha version, NOAA/Geophysical Fluid Dynamics Laboratory, Princeton, 580 pp., 1999.

Price, A. R., Voutchkov, I. I., Pound, G. E., Edwards, N. R., Lenton, T. M., and Cox, S. J.: Multiobjective tuning of Grid-enabled Earth System Models using a Non-dominated Sorting Genetic Algorithm (NSGA-II), in: Proceedings of the 2nd International Conference on eScience and Grid Computing, Amsterdam, Netherlands, p. 117, 2006.

Ridgwell, A.: Interpreting transient carbonate compensation depth changes by marine sediment core modeling, Paleoceanography, 22, PA4102, doi:10.1029/2006PA001372, 2007.

Ridgwell, A., Hargreaves, J. C., Edwards, N. R., Annan, J. D., Lenton, T. M., Marsh, R., Yool, A., and Watson, A.: Marine geochemical data assimilation in an efficient earth system model of global biogeochemical cycling, Biogeosciences, 4, 87–104, 2007,
http://www.biogeosciences.net/4/87/2007/.

Riebesell, U., Wolf-Gladrow, D. A., and Smetacek, V.: Carbon dioxide limitation of marine phytoplankton growth rates, Nature, 361, 249–251, 1993.

Sabine, C. L., Feeley, R. A., Gruber, N., Key, R. M., Lee, K., Bullister, J. L., Wanninkhof, R., Wong, C. S., Wallace, D. W. R., Tilbrook, B., Millero, F. J., Peng, T.-H., Kozyr, A., Ono, T., and Rios, A. F.: The oceanic sink for anthropogenic CO_2, Science, 305, 367–371, 2004.

Sarmiento, J. L., Orr, J. C., and Siegenthaler, U.: A perturbation simulation of CO_2 uptake in an ocean general circulation model, J. Geophys. Res., 97(C3), 3621–3646, 1992.

Schlitzer, R.: Carbon export in the Southern Ocean: Results from inverse modeling and comparison with satellite-based estimates, Deep Sea Res. II, 49, 1623–1644, 2002.

Schmittner, A., Oschlies, A., Giraud, X., Eby, M., and Simmons, H. L.: A global model of the marine ecosystem for long-term simulations: Sensitivity to ocean mixing, buoyancy forcing, particle sinking, and dissolved organic matter cycling, Global Biogeochem. Cy., 19, GB3004, doi:10.1029/2004GB002283, 2005.

Sjoberg, B. and Stigerbrandt, A.: Computations of the geographical distribution of the energy flux to mixing processes via internal tides and the associated vertical circulation in the ocean, Deep-Sea Res., 39(2A), 269–292, 1992.

Sverdrup, H. U.: On conditions for the vernal blooming of phytoplankton, Journal de Conseil Permanent International pour l'Exploration de la Mer, 18, 287–295, 1953.

Sweeney, C., Gloor, M., Jacobson, A., Key, R., McKinley, G., Sarmiento, J., and Wanninkhof, R.: Constraining global air-sea gas exchange for CO_2 with recent bomb ^{14}C measurements, Global Biogeochem. Cy., 21, GB2015, doi:10.1029/2006GB002784, 2007.

Wanninkhof, R.: Relationship between wind speed and gas exchange over the ocean, J. Geophys. Res., 97(C5), 7373–7383, 1992.

Weaver, A., Eby, M., Wiebe, E. C., Bitz, C. M., Duffy, P. B., Ewen, T. L., Fanning, A. F., Holland, M. M., MacFadyen, A., Matthews, H. D., Meissner, K. J., Saenko, O., Schmittner, A., Wang, H., and Yoshimori, M.: The UVic earth system climate model: Model description, climatology, and applications to past, present and future climates, Atmos. Ocean, 39, 1713–1724, 2001.

Willey, D. A., Fine, R. A., Sonnerup, R., Bullister, J. L., Smethie, M. W., and Warner, M. J.: Global oceanic chlorofluorocarbon inventory, Geophys. Res. Lett., 31, L01303, doi:10.1029/2003GL018816, 2004.